

# Wave modulation and wave sources in the solar convection zone

M. Kiefer<sup>1,\*</sup>, M. Stix<sup>1</sup>, and H. Balthasar<sup>2</sup>

<sup>1</sup> Kiepenheuer-Institut für Sonnenphysik, Schöneckstrasse 6, 79104 Freiburg, Germany (kief, stix@kis.uni-freiburg.de)

<sup>2</sup> Astrophysikalisches Institut Potsdam, Telegrafenberg, 14473 Potsdam, Germany (hbalthasar@aip.de)

Received 21 December 1999 / Accepted 18 May 2000

**Abstract.** We investigate the behavior of upward running sound waves in the lower photosphere by means of a 2-hour time series of FPI-filtergrams and a corresponding series of white-light images. From the FPI-filtergrams we obtain velocities in two heights in the solar photosphere. Using specific filters in the  $k_h$ - $\nu$ -space, we extract running sound waves from the velocity time series and the granulation from the white-light series. The relation between granular structure and wave amplitude is examined. To this end the granulation images are subdivided into intensity classes. The amplitudes of the waves are extracted on the pixel maps corresponding to these classes. We find hints for wave modulation due to the inhomogeneities in the solar convection zone: The behavior of the wave amplitudes meets theoretical predictions with respect to frequency- and height-dependence. The dependence on the horizontal wave number meets the predictions too, but due to low wave coherence at high wave numbers no definitive statement is possible. Further the darkest locations in the granulation are preferred by waves of increased amplitudes. There also seems to be a preference for the brightest granular regions. In both cases the behavior of the waves can be well described by subsurface sound sources. This is confirmed by comparison of the data with a simple model of a subsurface sound source.

**Key words:** Sun: granulation – Sun: oscillations – convection – waves

## 1. Introduction

The outermost layer of the solar convection zone is characterized by substantial inhomogeneities in the state variables, e.g. the temperature, and in the velocity field. This statement is obtained from a variety of models of convective energy transport, reaching from simple mixing-length models (e.g. Table 6.1 in Stix (1991)) to 3-D numerical simulations (Kim & Chan, 1998; Stein & Nordlund, 1998). From these one would expect that the influence of the convection structure on wave propagation is

strongest in a shallow layer of some 100 km thickness just below the visible solar surface.

The inhomogeneities in the velocity field might have an effect on the propagation of sound waves. This was first examined by Brown (1984) who found a decrease of the  $p$ -mode frequencies. Zhugzhda & Stix (1994) considered the propagation of radial sound waves in the solar convection zone by means of a discontinuous 2D two-layer model. They took into account the fluctuations of velocity and temperature by modeling the convection zone by alternating channels and predicted a decrease of  $p$ -mode frequencies too. Stix & Zhugzhda (1996) showed that there is a frequency-dependent modulation of the wave amplitude by the channels. The modulation should be best visible in upward running waves. Stix & Zhugzhda (1998) presented a 2D harmonic model of the convection zone with variations of velocity and sound speed. Again a  $p$ -mode frequency decrease was predicted. In the present work we shall show in Sect. 2.1 that for this model there are modulation effects similar to those of the discontinuous model.

The excitation of waves by the velocity field might be due to Reynolds-stresses within the turbulent convection field (e.g. Goldreich et al., 1994) or to the dynamic effects during the formation of downdrafts (e.g. Rast, 1999). Both effects place the level of sound-wave excitation at a depth of the order of 100 km below the surface of the Sun. Using data of Doppler velocity in several heights in the photosphere, Rimmele et al. (1995) found acoustic events in a frequency band around 3 mHz, located preferentially in intergranular lanes. Goode et al. (1998) used the same data and extended the analysis adding up intensity images at locations where acoustic events take place and found that these in fact prefer the dark intergranular space. Espagnet et al. (1996) used intensity and velocity data to examine relations between oscillations and granulation. They separated oscillations and granulation by filtering in the  $k_h$ - $\nu$ -space and found that oscillations at about 3 mHz clearly prefer the darkest regions. At 4 mHz and at 5 mHz no preference for any granular intensity level is indicated. At about 6 mHz there is again a preference of the dark granular regions by the oscillations.

In the present work we shall focus our attention on the behavior of photospheric running sound waves extracted from velocity data. The modulation effects should be best visible in such waves since they are not reflected but rather propagate

---

Send offprint requests to: M. Kiefer (Michael.Kiefer@imk.fzk.de)

\* Present address: Institut für Meteorologie und Klimaforschung, Forschungszentrum Karlsruhe GmbH, Postfach 3640, 76021 Karlsruhe, Germany

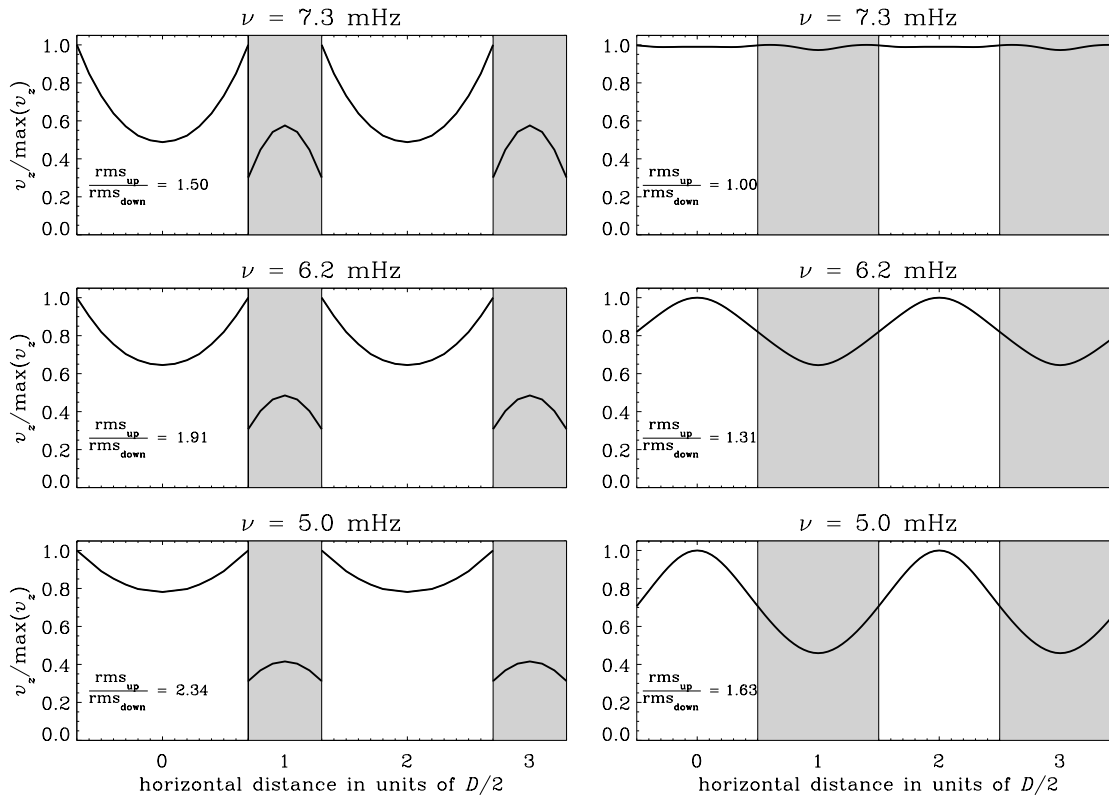


**Fig. 1.** Horizontal course of the normalized amplitude of the vertical velocity,  $v_z/\max(v_z)$  (thick curves), from the discontinuous 2D two-layer model of Zhugzhda & Stix (1994) (left column) and from the 2D harmonic model of Stix & Zhugzhda (1998) (right column), for three frequencies in the range of photospheric vertically propagating sound waves.  $D$  is the horizontal period of the inhomogeneities in the discontinuous and harmonic model, respectively. Shaded areas indicate the region of cool, downward flowing material. The ratio of the rms-amplitudes of  $v_z$  between regions with upstream and regions with downstream is given in each panel.

on through the photosphere. We first consider theoretically the modulation of running sound waves in the outer solar convection zone, by means of two 2D models (Zhugzhda & Stix, 1994; Stix & Zhugzhda, 1998). Apart from the wave modulation we expect to see the impact of local sound sources in our data. This is suggested by the results of Rimmele et al. (1995), although we shall use a frequency band well above 3 mHz. It is only reasonable to assume that the impact of acoustic events is not restricted to frequencies of about 3 mHz. Hence we attempt to give a simplified description of the wave field excited by a subsurface sound source.

## 2. Models and theoretical considerations

### 2.1. 2D models of the convection zone

Zhugzhda & Stix (1994) examined the propagation of radial sound waves in a 2D two-layer model with alternating channels of hot, upflowing and cool, downflowing material. The vertical velocity amplitude  $v_z$  of the waves varies over these channels, as demonstrated by Stix & Zhugzhda (1996) for the frequencies 3–9 mHz. This amplitude modulation increases with decreasing frequency. In the left column of Fig. 1 we present the normalized values of  $v_z$  for the frequencies 5, 6.2, and 7.3 mHz for the discontinuous model. In this frequency range, which cor-

responds to photospheric vertically propagating sound waves,  $v_z$  is larger in the bright upflow channels, but the ratio of  $v_z$  in the upflow channels to  $v_z$  in the downflow channels decreases with increasing frequency. To quantify this behavior we give the ratio of the rms-amplitudes of  $v_z$  between upstream and downstream channels in the pictures. Between 5 mHz and 7.3 mHz the change of this ratio is considerable; it should be detectable with modern techniques.

The propagation of sound waves with arbitrary horizontal wave number was examined by Stix & Zhugzhda (1998) in a second model where the course of the up- and downward velocities and of the squared sound speed was assumed to be harmonic. In this model the upflow and downflow regions have equal width. In the right column of Fig. 1 we show the wave amplitude  $v_z$  for the same three frequencies as for the discontinuous model. For this example the amplitudes of the velocity and squared sound speed are  $\Delta = 0.09$  and  $\delta = 0.245$ , cf. Eqs. (1) and (2) of Stix & Zhugzhda (1998), which is the closest approximation of the harmonic model to the discontinuous model. Again the modulation of  $v_z$  decreases with increasing frequency, at least in the frequency range treated here. The relative change of  $\text{rms}_{\text{up}}/\text{rms}_{\text{down}}$  between 5 mHz and 7.3 mHz is as large as in the discontinuous model. The absolute values of these ratios are closer to 1 and probably more realistic because of the

absence of discontinuities. Further calculations with the harmonic model (Stix, 2000) show that at still higher frequencies the wave amplitude becomes larger in the *dark* channels; for the granular structure considered in the present paper the transition occurs near 7 mHz, as one may expect from the right column of Fig. 1. In any case, as for the discontinuous model, we conclude that it should be possible to detect the differences in the wave amplitudes.

Now we want to give a plausible argument for a certain height dependence of the modulation effects in the lower photosphere. We imagine radially propagating plane waves to enter the layer where the horizontal inhomogeneities in sound velocity and flow field are strong. In passing this layer the waves are modulated and presumably also diffracted, i.e. their surfaces of constant phase are deformed depending on the local properties of the ambient medium. The photosphere itself is dominated by radiative processes; therefore the horizontal temperature inhomogeneities are efficiently diminished. On the other hand, the velocity pattern persists as overshooting over several 100 km. Therefore we expect some further enhancement, or at least no decrease, of the degree of modulation in the lower photosphere.

What kind of dependence of the ratio of the wave amplitudes on the horizontal wave number  $k_h$  do we expect? Two types of inhomogeneities are of importance for the wave modulation. The first, and probably major, is the horizontally varying ratio of convective velocity to sound speed at constant depth. The second is the ratio of convective temperature excess to the average temperature. From a standard solar model with mixing-length prescription of the convection (e.g. Kiefer et al. (2000)), we take the following estimates: The relative temperature excess and velocity ratio both peak at less than 100 km depth below the solar surface ( $\tau_{500} = 1$ ) with peak values of order 30%. At 200 km depth the temperature excess is approx. 10% while the convective velocity still reaches about 20% of the sound velocity. At 1000 km below the surface the values are 1% and 10% for the temperature and velocity inhomogeneities, respectively. Hence the influence of the convective structure on the wave propagation might well reach down to 1000 km or more. The horizontal scale of the convective structure is of the same order of magnitude (at the surface 1000 km is a typical scale in the granulation). The convective up- and downdrafts are predominantly aligned to the gravity, while the direction of propagation of sound waves is given by the ratio of horizontal to vertical wave number. With the standard solar model we estimated the vertical wave number, using the dispersion relation for waves in a stratified isothermal atmosphere (e.g. chapter 5 of Stix (1991)). For a frequency of 6 mHz, which in the photosphere and below corresponds to running sound waves, we calculated the angles  $\theta$  with respect to the radial direction in the region between the solar surface and 1000 km depth; We obtained  $\theta \approx 5^\circ$  for  $k_h = 0.15 \text{ Mm}^{-1}$ ,  $\theta \approx 15^\circ$  for  $k_h = 1.5 \text{ Mm}^{-1}$ ,  $\theta \approx 30^\circ$  for  $k_h = 2.5 \text{ Mm}^{-1}$ , and  $\theta \approx 45^\circ$  for  $k_h = 3.5 \text{ Mm}^{-1}$ . For a wave with small  $k_h$  the modulation at any point on the solar surface will be caused essentially by only a single “channel”, since during the propagation through the depth range of 1000 km the wave mostly remains in the same convective flow regime, either up- or down-

draft. The influence of the convective inhomogeneities will be a maximum in this case. On the other hand, a wave with large  $k_h$ , in particular for  $\theta \geq 45^\circ$ , will experience the influence of varying convective flow regimes, and we expect less modulation visible at the surface.

To summarize the conclusions from the models and from physical arguments: As far as wave *modulation* is concerned, we expect the following dependences of the ratio of the wave amplitudes between hot upflow and cool downflow regions: A decrease of the ratio with increasing wave frequency, an increase, or at least no decrease, with increasing height in the lower photosphere, and a decrease of the ratio with increasing horizontal wave number.

## 2.2. A simple model of a subsurface sound source

Since subsurface sound sources can be expected to influence the behavior of running sound waves with respect to the granular structure we constructed a simple model of a subsurface sound source. Again only waves with frequencies above the atmospheric cutoff frequency are considered to avoid the impact of reflected waves. We take two steps to compare the model and the analyses of the observations: First we define the source *per se*, second we give a prescription of how to convert the model data to synthetic observations which could be compared with our observational data.

We made the following assumptions to define the source:

- Sources are isolated, i.e. their velocity fields do not significantly interfere.
- The wave field of the source is axisymmetric about an axis perpendicular to the (plane) solar surface (Fig. 2).
- The atmosphere is isothermal. Above the atmospheric cutoff frequency the influence of the atmospheric stratification on the height dependence of the wave amplitude is the same as for vertically propagating plane waves.
- At every given frequency there is a background of waves which we shall regard as upward propagating plane waves. Since these waves originate from different locations and times they might be reasonably assumed to be uncorrelated. Therefore the phases of the waves from the sound source and of the background plane waves are uncorrelated too.
- The power of the background plane waves is equally distributed over all locations, regardless of the granular pattern. This means that in our sound-source model there are no effects of wave modulation.

Since we intend to look at amplitude ratios we do not need absolute amplitudes, neither for the background waves nor for the sound source itself. We rather shall choose a ratio of these two quantities that gives a result in rough accordance with the observations.

According to the scenario of Rast (1999) the sound source is modelled to have an approximately multipolar wave field. The velocity potential of the wave field depends on the spherical polar angle  $\theta$  and the distance  $s$  from the source center (Fig. 2) like

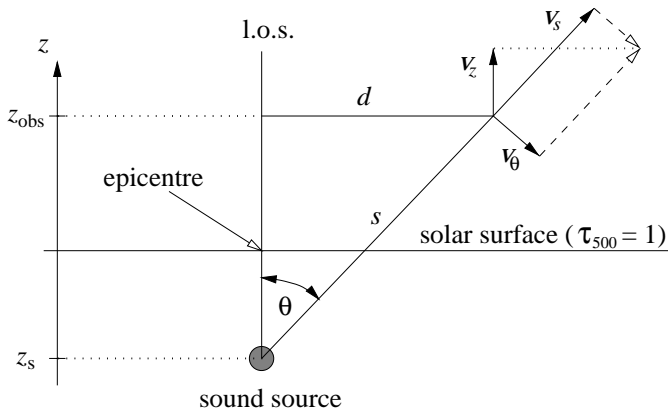


**Fig. 2.** Geometric quantities for the calculation of the vertical velocity  $v_z$  of a subsurface sound source. The line of sight (l.o.s.) is orthogonal to the solar surface, corresponding to our disc-center observations.

$$\psi_{l,n} \propto P_l(\theta) s^{-n}, \quad \text{with } n, l \text{ integers.} \quad (1)$$

Here  $P_l(\theta)$  is the Legendre polynomial of degree  $l$ . This is a pure mathematical definition since  $\psi_{l,n}$  is not a solution to the Helmholtz-equation (Landau & Lifshitz, 1963); especially there is a singularity at the origin. However, this does no harm to our application because the origin is assumed to be below the solar surface in our model.

From the geometric quantities explained in Fig. 2 and from Eq. (1) the amplitude  $v_z$  of the vertical velocity of the wave field at a given height  $z_{\text{obs}}$  and a given distance  $d$  from the epicenter can be calculated. It is obvious from (1) that the amplitude  $v_z$  decreases for increasing  $z_{\text{obs}}$  as well as for increasing  $d$ .

The method to convert the model data to synthetic observations will be explained in Sect. 5.2.

### 3. Observation and data preparation

The data were taken on July 6, 1996 at the German Vacuum Tower Telescope at the Observatorio del Teide, Tenerife. A field of  $76'' \times 55''$  of magnetically quiet Sun at disc center was observed for 119 min with the CCD cameras CCD1 and CCD2 of the 2D-spectrometer of the Göttingen University (Bendlin & Volkmer, 1995). The pixel size corresponds to  $0''.2 \times 0''.2$ . The initial data consist of two strictly simultaneous series of 160 temporally equidistant blocks of 40 images each. The blocks of the first series consist of 40 white-light images, the blocks of the second one consist of 40 filtergrams with wavelength steps of 1.786 pm around the absorption line of Fe I at 709.04 nm. The recording of a block took 11 s, the time from block to block was 44.8 s. Seeing conditions ranged from moderate to good during the observation.

After dark and gain table corrections of the white-light and filtergram series, image motion and distortion were determined from the images of the white-light series. Since filtergrams and white-light images were taken simultaneously, the resulting corrections could be applied directly to the former. The corrections reduced the image size to  $65'' \times 43''$ .

One data set was extracted from the  $160 \times 40$  white-light images. It consists of the respective best image of each block, which gives a series of 160 images, not perfectly equidistant in time. This series will be called  $I_B$  in what follows.

The 40 filtergrams allowed to reconstruct the absorption profile of the Fe I line for each pixel in the image separately. After application of an optimal filter we extracted the line-of-sight Doppler velocity at the line core and at a line depression of 20%. The intensity contribution functions corresponding to these two positions have their center of gravity at approximately 50 km and 250 km above  $\tau_{500} = 1$ , respectively. We shall regard 50 km and 250 km as approximate values for the heights of the velocity signals from 20% line depression and from the line core, respectively. The corresponding time series of dopplergrams will henceforth be called  $v_{50}$  and  $v_{250}$ . These series are used to extract amplitudes of the vertical velocity for running sound waves in several frequency bands.

Table 1 gives a list of name, content, and purpose of the three time series used for the further analyses.

### 4. Power in the diagnostic diagram and data filtering

Time series of the intensity and of the vertical velocity component from the photosphere contain signatures of granulation, oscillations corresponding to standing waves, namely the  $p$ -modes and the f-mode, and oscillations representing running sound waves and running gravity waves. In order to analyze these distinct phenomena we separate them by means of filters in the Fourier domain of the space-time domain  $(x, y, t)$ , the  $(k_x, k_y, \omega)$ -space. We shall use the term  $k_h$ - $\nu$ -space in what follows, with  $k_h = (k_x^2 + k_y^2)^{1/2}$  and  $\nu = \omega/2\pi$ .

For the identification of running sound waves and of granulation in the  $k_h$ - $\nu$ -space we first Fourier transformed the data series  $I_B$ ,  $v_{50}$ , and  $v_{250}$ , and then calculated spectra of power, phase-difference, and coherence in the  $k_h$ - $\nu$ -plane (e.g. Deubner et al. (1992)), using Hanning windows for space and time apodization. The power spectra for  $I_B$  and  $v_{250}$  are shown in Fig. 3. The power spectrum of  $v_{50}$  is not markedly different from the one of  $v_{250}$  and is therefore not presented.

From inspection of the power spectrum of the white-light data series it becomes clear that there is no distinct feature which allows to separate granulation from oscillations. Moreover there is no physical reason for the granulation power to be restricted to a certain area in the  $k_h$ - $\nu$ -plane. Therefore we *define* the region of granulation in the  $k_h$ - $\nu$ -plane to lie outside the area of evanescent oscillations and somewhat below the acoustic cut-off frequency  $\nu_{\text{ac}}$ . The latter is approximately  $\nu_{\text{ac}} = 5$  mHz for lower photospheric conditions. Above  $\nu_{\text{ac}}$  the atmosphere supports propagating sound waves. Their location in the  $k_h$ - $\nu$ -plane can be approximated by the area above the acoustic branch of the dispersion relation for an isothermal atmosphere (Stix, 1991, Sect. 5.2). Here we approximate this branch by the two lines  $\nu = \frac{1}{2\pi} c_s k_h$  and  $\nu = 4.5$  mHz. The reason for the latter choice is that in the phase-difference spectra there are already phase differences of  $5$ – $10^\circ$  between  $v_{50}$  and  $v_{250}$  at this frequency. Above  $\nu = 5$  mHz the phase differences reach  $20$ –

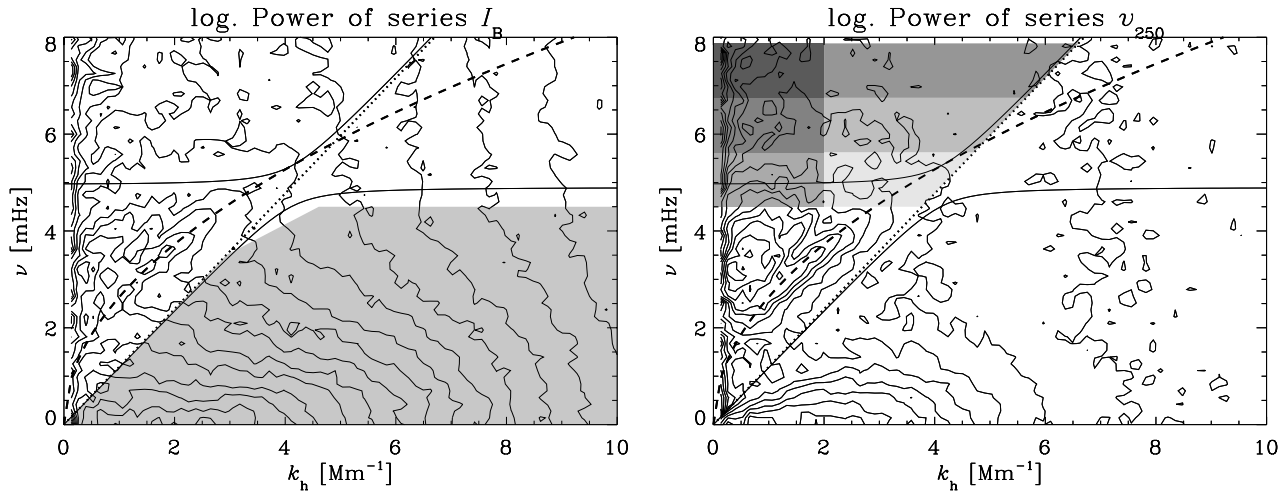


**Fig. 3.** Power of series  $I_B$  (left) and  $v_{250}$  (right) in the diagnostic diagram. Isocontours are separated by a factor of  $\sqrt{10}$ . Dotted line: Lamb mode with  $\nu = \frac{1}{2\pi} c_s k_h$ , for  $c_s = 7.5 \text{ km s}^{-1}$ . Heavy broken curve: dispersion relation for surface waves,  $\nu = \frac{1}{2\pi} \sqrt{g k_h}$ , with  $g = 274 \text{ m/s}^2$ . Shaded areas outline the filters for the granulation (left) and for the running sound waves (right).

**Table 1.** The three time series used in this work

name	content of time series	purpose
$I_B$	best white-light images of scans	definition of granulation structure
$v_{50}$	Doppler velocity from the line wings	velocity amplitude of waves from a layer around 50 km above $\tau_{500} = 1$
$v_{250}$	Doppler velocity from the line core	velocity amplitude of waves from a layer around 250 km above $\tau_{500} = 1$

$30^\circ$ . These positive phase differences indicate the existence of upward running sound waves in this region of the  $k_h$ - $\nu$ -plane. The coherence between  $v_{50}$  and  $v_{250}$  (not shown here) breaks down above  $k_h \approx 2 \text{ Mm}^{-1}$ . We took this line as a boundary, but did not discard the data above  $k_h = 2 \text{ Mm}^{-1}$ . We rather distinguish between sound waves within the theoretical limit and sound waves restricted by  $k_h < 2 \text{ Mm}^{-1}$ .

Fig. 3 shows the contours of the used filters as shaded areas. The region of running sound waves was further subdivided into the frequency ranges 4.5–5.625 mHz, 5.625–6.75 mHz, and 6.75–7.875 mHz. This is to examine a possible frequency dependence of the relations between granulation and waves. The definition of the filter contours and the designation  $K_F$  of the filters is given in Table 2. All edges of the filters were smoothed to reduce ringing effects. An apodization was applied to 10% of the data at each border of the two spatial and the temporal domains. After Fourier transformation the data were multiplied by the filter function, transformed back and divided by the apodization function. At each border 5% of the resulting data were cut off, which left data sets of spatial dimensions  $59'' \times 39''$  and duration 107 min. The granulation filter was applied to the series  $I_B$ , the six oscillation filters were applied to the series  $v_{50}$  and  $v_{250}$ .

After the filtering we had thirteen time series: one series of the granulation structure in white-light data, filtered with  $K_F = 40$ , three series of upward running sound waves, filtered with  $K_F = 56, 57, 58$ , for each of the two height layers at 50 km and 250 km, and three series of upward running sound waves, filtered with  $K_F = 561, 571, 581$ , with  $k_h < 2 \text{ Mm}^{-1}$ ,

also for both height layers. The twelve oscillation series allow to examine the dependence of the wave behavior on frequency and, to some extent, height and wave number.

## 5. Methods of data analysis

### 5.1. Relations between running sound waves and granulation

As in Kiefer & Balthasar (1998) we defined ten pixel classes based on intensity values to extract granulation features from the series  $I_B$ , filtered with  $K_F = 40$ . The pixel classes are indicated either by an index  $i = 1 \dots 10$ , or by their relative intensity range  $[(i-1)/10, i/10)$ . In the first class,  $[0, 0.1)$ , there are the ten percent darkest pixels, in the class  $[0.1, 0.2)$  the pixels for which 10% of all pixels are darker and 80% of all pixels are brighter, and so on. The index  $m$  designates the image number within the time series.

We calculated the ratio  $v_{A,m,i}$  between the rms wave amplitude in a pixel class  $i$  and the average rms wave amplitude of all classes within an image  $m$ . Then the mean  $\langle v_A \rangle_i$  of  $v_{A,m,i}$  over all  $M$  images of the time series was calculated. In what follows we shall omit the indices and simply write  $v_A$  and  $\langle v_A \rangle$ . Since  $\langle v_A \rangle$  depends on the intensity class, a value greater than one within an intensity class means a preference of the corresponding granular regions either by waves in general or by waves with higher than average amplitude.

An estimate for the statistical significance is Student's  $t$ ,

$$t = \frac{|\langle v_A \rangle - 1|}{\delta v_A} \sqrt{n},$$

**Table 2.** The filters for granulation and running sound waves in the  $k_h$ - $\nu$  plane (sound velocity  $c_s = 7.5 \text{ km s}^{-1}$ )

$K_F$	content	definition of boundaries in the $k_h$ - $\nu$ plane	
40	granulation	$\nu < 4.5 \text{ mHz}$	and $\nu < \frac{1}{2\pi} c_s k_h$ and $\nu < \frac{1}{4\pi} c_s k_h + 1.75 \text{ mHz}$
56	running sound waves	$4.5 \text{ mHz} < \nu < 5.625 \text{ mHz}$	and $\nu > \frac{1}{2\pi} c_s k_h$
57	running sound waves	$5.625 \text{ mHz} < \nu < 6.75 \text{ mHz}$	and $\nu > \frac{1}{2\pi} c_s k_h$
58	running sound waves	$6.75 \text{ mHz} < \nu < 7.875 \text{ mHz}$	and $\nu > \frac{1}{2\pi} c_s k_h$
561	running sound waves	$4.5 \text{ mHz} < \nu < 5.625 \text{ mHz}$	and $k_h < 2 \text{ Mm}^{-1}$
571	running sound waves	$5.625 \text{ mHz} < \nu < 6.75 \text{ mHz}$	and $k_h < 2 \text{ Mm}^{-1}$
581	running sound waves	$6.75 \text{ mHz} < \nu < 7.875 \text{ mHz}$	and $k_h < 2 \text{ Mm}^{-1}$

(e.g., Fisher 1950) for normally distributed  $v_A$  with expectation value  $\langle v_A \rangle = 1$ . Actually the distribution of  $v_A$  is close to normal within each intensity class (Kiefer, 1999). Here  $n$  is the degree of freedom of the series and  $\delta v_A$  is the standard deviation. The degree of freedom is essentially equivalent to the number of independent measurements. For impulsive events which can be assumed independent of each other the typical time scale might be of the order of five minutes (Rimmele et al., 1995), which gives  $n \approx 20$  for 107 min observation time. If one regards the granulation pattern as the defining agent for the time scale, only a few independent observations are made (granular lifetime is approximately 20 min, therefore  $n \approx 5$ ). For 99% confidence the values of  $t$  are 2.85 ( $n = 20$ ) and 4.03 ( $n = 5$ ). Hence we shall consider values of  $t > 4$  as an indication for significant deviations of  $\langle v_A \rangle$  from 1.

### 5.2. Radial distribution of intensity classes for the generation of synthetic observations

To convert the velocity field of the sound source model presented in Sect. 2.2 into synthetic observations we must know the distribution of intensity classes around the epicenter. To simplify matters we assumed that the sound sources are located only within a limited number of intensity classes. For the present analyses we took the classes 1 and 10.

Taking the images of series  $I_B$  we regarded all single pixels of the particular intensity classes 1 or 10 as possible epicenters. A series of concentric annuli with increasing radii  $d_j$  and constant width  $0''.2$  around all these pixels was used to find the relative frequency  $h_i(d_j)$  of pixels in intensity class  $i$  at distance  $d_j$  from the epicenter.

From  $v_z$  of the model and from  $h_i(d_j)$  a quantity that corresponds to  $\langle v_A \rangle$  was calculated. This quantity will be called  $e_i$ . For the model we took  $l = 1$  and  $n = 1$  and assumed a depth of the source of  $z_s = 200 \text{ km}$ . Actually the values for  $e_i$  do not strongly depend on these choices.

Fig. 4a shows  $h_i(d)$  for epicenters located in regions corresponding to the ten percent darkest pixels, i.e., intensity class  $i = 1$ . The curve labeled [0, 0.1) gives  $h_1(d)$ , i.e., the probability of finding a pixel of the class [0, 0.1) at distance  $d$  from the epicenter. The probability is 1 at the origin since the epicenter itself is in this class. Likewise the probability for any other class is zero there. With increasing  $d$  the probability for the class  $i = 1$  decreases monotonously while the relative frequencies for all

other classes increase. Up to  $d \approx 1''.5$  it is always more likely to find class  $i$  than to find class  $i + 1$ : in the neighborhood of darkest pixels there are most likely darkest pixels, then quite dark pixels, then dark pixels, and so on. At approx.  $2''$  all ten curves meet at a value of 1/10.

The behavior of  $h_i(d)$  for epicenters in the brightest regions (Fig. 4b) is similar at first glance. However, there are differences: The probability to find brightest pixels around brightest centers sinks somewhat faster with increasing  $d$  and falls below 1/10 beyond  $1''$ . This means that the average bright granule is surrounded by darker material. Again at  $2''$  all ten curves meet.

So, are very dark regions more extended than very bright ones? That would be in contrast to the observations that typical bright granules are more extended than typical dark intergranular regions. The brightest regions are made up mostly of granule centers and are of roundish shape. These are surrounded by darker material, often in the form of a dark closed intergranular lane. On the other hand the darkest regions often occur where several intergranular lanes meet. Therefore the probability to find a still very dark location at a moderate distance from a dark center is higher than the probability to find a bright region around a bright center. A second question is whether our analysis indicates that granules have a diameter of  $2''$ . In Fig. 4b we show the values of  $h_i(d)$  for epicenters in the very brightest regions. The brightest locations usually correspond to centers of large granules. Therefore a diameter of  $2''$  is not unlikely for these epicenters. Of course this case is not representative for all granules.

## 6. Results and discussion

In Fig. 5 the results of the model calculations and of the analysis of the observations are compiled. Fig. 5a shows values of  $e_i$  for  $i = 1$ , in which case the epicenters are located in regions corresponding to the ten percent darkest granular features, while Fig. 5b shows  $e_i$  for the superposition of wave fields of sources in the darkest regions and somewhat weaker sources in the brightest regions. The amplitude ratio of the sound source and of the background waves was arbitrarily set to a value that gave a result that was in rough agreement with the results of the data analyses.

In the Figs. 5c–h the values of  $\langle v_A \rangle$  and the corresponding values of Student's  $t$  are depicted. The left column of the ob-

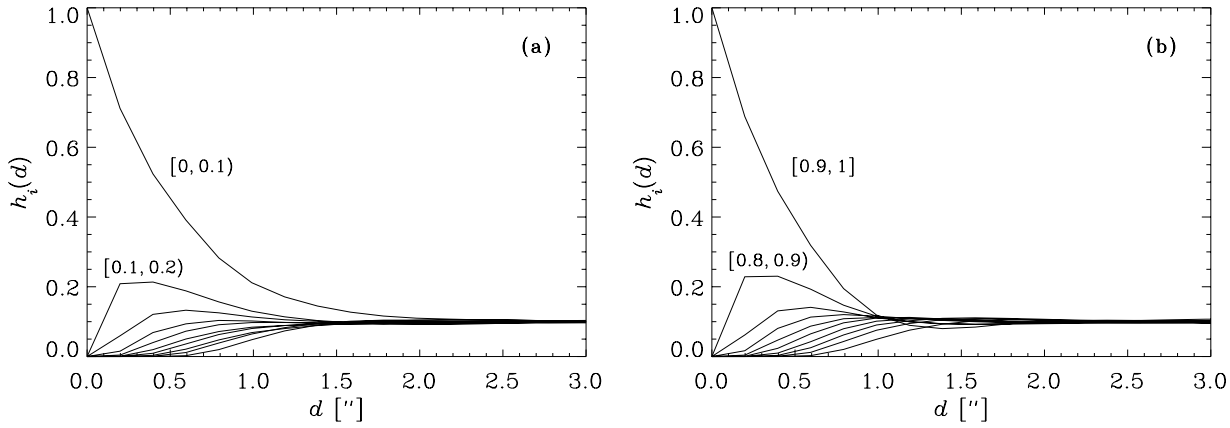


**Fig. 4a and b.** Relative frequency  $h_i(d_j)$  for the occurrence of the intensity class  $i$  on an annulus of radius  $d_j$  and width  $0.2$  around epicenters located in intensity classes 1 **a** and 10 **b**. To improve the visualization  $d_j$  is represented by the continuous value  $d$ . Some  $h_i$  curves are labeled by the intensity classes.

servational analyses, Figs. 5c,e,g, represents the results for the filters  $K_F = 56, 57, 58$ .

The following discussion of the diverse results will be separated into two parts. The first part deals with the comparison of synthetic and real observations, while the second concentrates on how  $\langle v_A \rangle$  depends on observation height, frequency, and wave number. Of course the two parts cannot be separated strictly, but the physical interpretation of the data suggests this division in a natural way.

### 6.1. Comparison of synthetic and real observations

For the oscillation series  $v_{50}$  from the lower observation height at approx. 50 km (thin, solid curves) the following can be seen: In general the run of  $e$  in Fig. 5b coincides roughly with that of  $\langle v_A \rangle$  for  $K_F = 56, 57, 58$ , i.e., for the waves only restricted by the Lamb mode. The corresponding value of Student's  $t$  indicates high significance in these cases. A closer look reveals that the coincidence between  $\langle v_A \rangle$  and  $e$  in Fig. 5a up to intensity class [0.6, 0.7] is even very good. Up to  $i = 7$  the model of sound sources only in the darkest granular regions gives a very satisfying description of the observations, while the model of sound sources in both extreme intensity classes performs not so well. In contrast, for the oscillation series  $v_{250}$  from the greater height at approx. 250 km (thick, solid curves) a systematic, frequency-dependent deviation is apparent, but apart from this the course of  $\langle v_A \rangle$  shows a moderately good coincidence with the simple model of subsurface sound sources. The deviation can roughly be regarded as a slope towards lower values at bright intensity classes. In Sect. 6.2 we shall discuss a possible reason for this.

The running sound waves obtained with  $K_F = 561, 571, 581$ , i.e., the waves restricted by a maximal wave number of  $2 \text{ Mm}^{-1}$ , show a much stronger deviation from the theoretical prediction of our source model. The course of  $\langle v_A \rangle$  for the data from 250 km never shows a significant similarity to that of  $e$ . In the lowest frequency band there is even a significant avoidance

of dark granular regions. The data from 50 km approximate the run of  $e$  the better the higher the wave frequency is.

From the comparison of the synthetic and real observations it is likely that subsurface sound sources indeed are located in the darkest granular regions. This result is in accord with the findings of Rimmele et al. (1995). Further there seems to be evidence for additional sound sources in the brightest regions of the granular structure. This type of sound source is only poorly modeled by our simple model. Judging from the different decay of  $\langle v_A \rangle$  from the extreme intensity classes towards less extreme ones we conclude that the depth of the sound sources in bright regions might be much less compared to sources in dark regions. A further interesting point is that in the  $v_{50}$  data filtered with  $K_F = 561, 571, 581$  the values of  $\langle v_A \rangle$  in the lowest intensity classes are in general less than those of the corresponding data filtered with  $K_F = 56, 57, 58$ . A possible explanation is that the sound sources are of such a small diameter that the wave number restriction  $k_h < 2 \text{ Mm}^{-1}$  already acts as a cut-off. This would imply that the typical diameter of the sound sources is less than  $2''/15$ . This is in agreement with the findings of Goode et al. (1998), who give a diameter of  $1''/4$  for their acoustic events. The fact that there is a scaling of the  $\langle v_A \rangle$  curves with frequency might be explained by this argument too. As can be seen from the right picture of Fig. 3, the higher the frequency is, the larger is the horizontal wave number for the filters  $K_F = 56, 57, 58$ . An increase of the wave number means that the size of features contained within the filtered data decreases. Therefore, if the sound sources are of small extent, they will show more influence in the data sets of high frequency.

### 6.2. Behavior of the running sound waves

#### 6.2.1. Dependence on frequency

As we have already mentioned in the preceding section, there is a frequency-dependent slope in the course of  $\langle v_A \rangle$  for the  $v_{250}$  data filtered with  $K_F = 56, 57, 58$ . Compared to the run of  $e$  in Fig. 5b the slope decreases with increasing frequency.

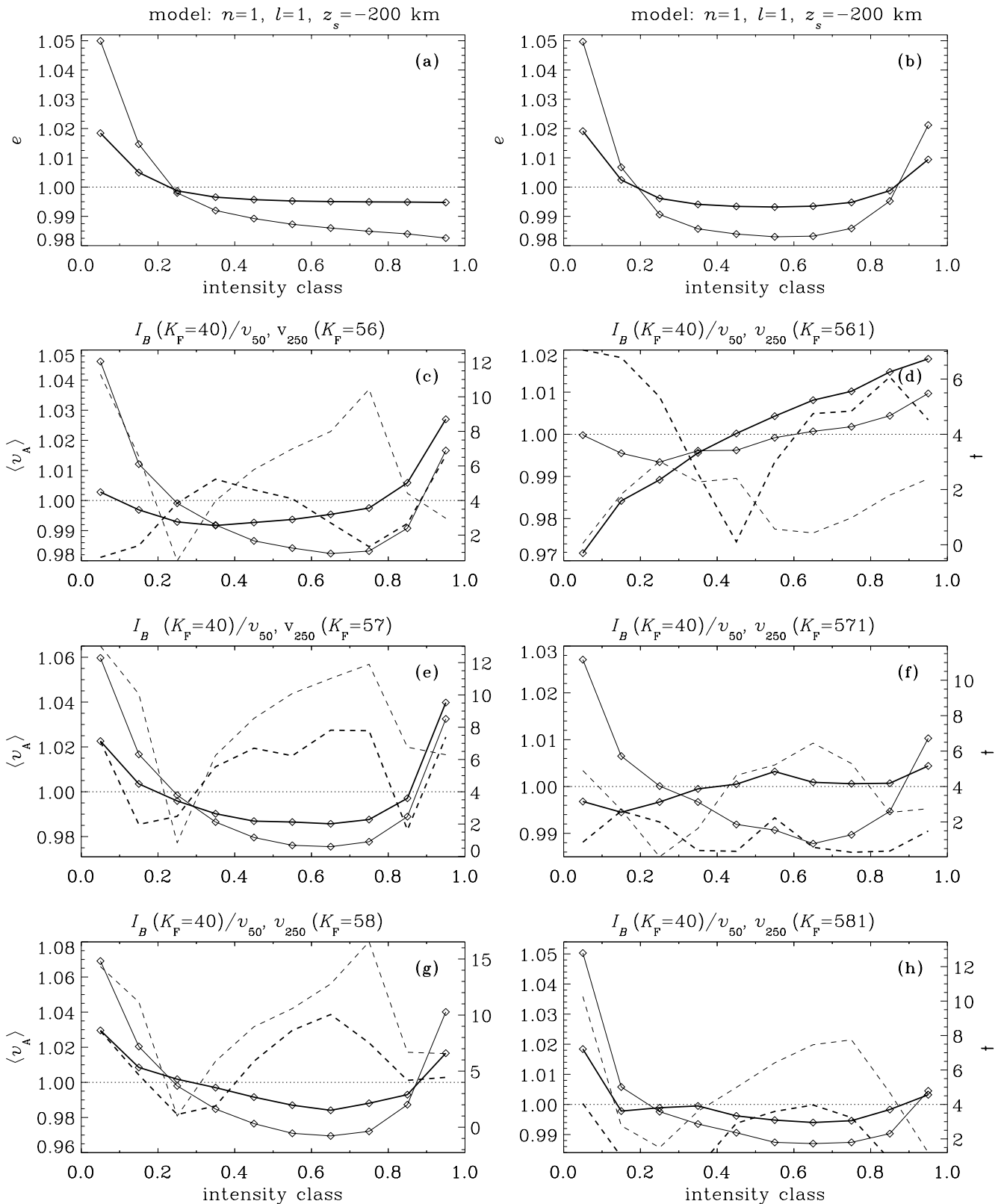


**Fig. 5a–h.** Amplitude ratio  $e$  from the localized-source model in the darkest (a) and in the darkest and brightest (b) regions of the granulation. In pictures (c)–(h) the average  $\langle v_A \rangle$  and the corresponding values of Student's  $t$  from our analysis of the observations are shown. Solid curves with diamonds correspond to  $e$  and  $\langle v_A \rangle$ , broken curves indicate  $t$ . Values from the height 50 km in the photosphere are marked with thin curves, while thick curves correspond to 250 km. The dotted line is at  $e = 1$  (a,b), and at  $\langle v_A \rangle = 1$  and  $t = 4$  (c–h); cf. Sect. 5.1 for the meaning of this special value of  $t$ . The ordinate axes all have individual scalings.

The corresponding  $v_{50}$  data show no perceptible slope or other deviations. The only dependence on frequency manifests itself in a slight scaling of  $\langle v_A \rangle$ .

A similar but much more pronounced behavior can be found in the  $v_{250}$  data filtered with  $K_F = 561, 571, 581$ . Here the slope dominates the course of  $\langle v_A \rangle$  for low frequency. The corresponding values of  $t$  indicate significance of the deviations from  $\langle v_A \rangle = 1$ . At intermediate frequencies there is no significant deviation, while at high frequencies the course of  $\langle v_A \rangle$  shows a tendency to assume the shape of the simple model of sound sources in either, darkest and brightest granular regions (Fig. 5b). But this is just a tendency, the values of  $\langle v_A \rangle$  are not significantly different from 1. A somewhat different behavior is shown by the  $v_{50}$  data filtered with  $K_F = 561, 571, 581$ . At low frequencies the  $\langle v_A \rangle$  curve does not significantly deviate from the value 1. Nevertheless there is a slope and a bending of the curve that makes it look like a scaled-down and inclined version of  $e$  in Fig. 5b. For intermediate frequencies the course of  $\langle v_A \rangle$  is quite similar to that for the  $v_{50}$  data filtered with  $K_F = 56, 57, 58$ . However, the significance is not as high as in that case. At the highest frequencies  $\langle v_A \rangle$  for  $v_{50}$  (Fig 5h) shows a significant deviation from 1. The form of the curve is moderately similar to that of  $e$  in Fig. 5b.

For the interpretation of these results we must not forget that the general behavior is a compound of several contributions. The most significant ones might be the impact of local sound sources and the modulation induced by the horizontal structure of the upper convection zone. The influence of the sound sources is strongly reduced with increasing height. Therefore it seems reasonable to concentrate on the behavior of  $v_{250}$  with respect to frequency changes when one wants to look for the effects of wave modulation. This behavior is in fact in good agreement with the theoretical predictions of Sect. 2.1. At low frequency the ratio of the rms velocities in the hot (bright) and cool (dark) channels (regions) is high, hence the modulation is well visible in  $\langle v_A \rangle$ . At high frequency this ratio diminishes, and consequently the modulation has less influence on  $\langle v_A \rangle$ . For  $v_{50}$  there is still a tendency to the same behavior, at least for data filtered with  $K_F = 561, 571, 581$ .

### 6.2.2. Dependence on height

The curves presented in Figs. 5c–h show that there is a difference between  $\langle v_A \rangle$  from  $v_{250}$  and from  $v_{50}$ . In the data filtered with  $K_F = 56, 57, 58$  the  $\langle v_A \rangle$  curves corresponding to the lower height of approx. 50 km do not show any variation apart from a scaling. The  $\langle v_A \rangle$  curves for  $v_{250}$  however vary. As already discussed in the preceding section, there is a slope of the curves, increasing with decreasing frequency.

The case is similar for the data filtered with  $K_F = 561, 571, 581$ . Here too the data from the greater height are much more influenced by frequency variations. Moreover, at low frequencies the course of  $\langle v_A \rangle$  looks like being generated solely by wave modulation. Dark regions have lower rms velocity-amplitudes than average, while bright regions have larger rms velocities.

Altogether the influence of the wave sources is high in the data from lower height and the impact of wave modulation is stronger in the data from greater height.

### 6.2.3. Dependence on wave number

The dependence on wave number is the most difficult topic of this discussion. This is because we actually did not separate the waves in  $k_h$  but rather use overlapping regions in the  $k_h$ - $\nu$  plane (see Table 2). Thus, the data filtered with  $K_F = 56, 57, 58$  contain all of the data filtered with  $K_F = 561, 571, 581$ , respectively. However, there are strong differences in the behavior of  $\langle v_A \rangle$  between these data sets.

At a first glance the curves for the data filtered with  $K_F = 56, 57, 58$ , i.e., waves only restricted by the Lamb mode  $\nu = \frac{1}{2\pi} c_s k_h$ , all roughly look similar, while those for the data filtered with  $K_F = 561, 571, 581$  show strong variations. A closer look reveals that some of the properties of the  $\langle v_A \rangle$  curves for the data filtered with  $K_F = 56, 57, 58$  can be ascribed to the behavior of the  $\langle v_A \rangle$  curves for the  $K_F = 561, 571, 581$  data. This is most clearly seen for the  $v_{250}$  series (thick solid curves). If one would subtract the  $\langle v_A \rangle$  curves for  $K_F = 561, 571, 581$  from the corresponding curves for  $K_F = 56, 57, 58$ , respectively, then the resulting curves would show a diminished dependence on frequency. We give two examples as illustrations. Firstly, if we look at the values of  $\langle v_A \rangle$  for the series  $v_{250}$  in the intensity class [0, 0.1), we can see that the difference between the two filter classes always amounts to approx. 0.02. Secondly, we note that the kink of the  $v_{250}$  curve at intensity class [0.3, 0.4) in Fig. 5h corresponds to a quite flat run of  $\langle v_A \rangle$  in Fig. 5g, compared to the curves in Figs. 5c,e. The behavior of  $\langle v_A \rangle$  in the intensity class [0.9, 1] does not support our view, but apart from this single point the general behavior of  $\langle v_A \rangle$  does. Now a simple subtraction is not perfectly suited for this argumentation, because the operations which lead to the  $\langle v_A \rangle$ -values are not all linear. On the other hand the deviations from 1 are not too large and therefore the subtraction might give an acceptable guess for the behavior of the  $v_{250}$ -data for waves which come from the region with  $k_h > 2 \text{ Mm}^{-1}$ .

Now we must not forget that the coherence spectra for  $v_{50}$  and  $v_{250}$  show low values above  $k_h$  approx.  $2 \text{ Mm}^{-1}$  in the frequency range of running sound waves (Sect. 4). A different explanation for the small wave modulation of the waves with  $k_h > 2 \text{ Mm}^{-1}$  therefore is that there are simply not enough coherent waves to show coherent modulation effects in both heights. Hence the dependence on wave number is the least certain effect discussed here.

## 7. Conclusions

The vertical velocity of upward propagating sound waves shows a characteristic amplitude distribution with respect to the granular structure, as given by the white-light intensity. The features of this distribution depend on the frequency, on the range of the horizontal wave number, and on the height in the photosphere.

We have discussed two theoretical models which are able to describe the larger part of the amplitude distribution:

A simple model of a subsurface sound source located in the darkest 10% of the granulation well represents the amplitude distribution of all running sound waves for dark and intermediate intensity classes. However, for the brighter intensity classes the distribution of wave amplitudes is not correctly predicted. Assuming additional sound sources in the brightest 10% of the granulation gives the rough shape of the observed distribution. Due to the simplicity of the sound-source model we are not able to give a sound estimate for the depth of sound sources below the solar surface. The assumed value of 200 km is in rough agreement with current estimates.

There is a deviation of the model data from the observations. This deviation depends on the frequency and horizontal wave number of the waves and on the photospheric height. These dependencies fit quite well with the results of 2D models of wave propagation in the convection zone and with the expectation of wave modulation from a physical reasoning.

Altogether we find hints that there exist local sound sources in the darkest granular regions, and possibly in the brightest regions too. Further there is some indication that wave modulation due to horizontal inhomogeneities in the convection zone influences the appearance of outward propagating waves in the solar photosphere.

*Acknowledgements.* We gratefully acknowledge useful discussions with W. Schmidt (KIS) and with Y. Zhugzhda (AIP). We thank H. Schleicher (KIS) for calculating the contribution functions for us. The referee's constructive comments helped to improve the paper. The VTT on Tenerife is operated by the Kiepenheuer-Institut für Sonnenphysik in

the Observatorio del Teide of the Instituto de Astrofísica de Canarias. The Göttingen 2D-spectrometer was supported by the *Deutsche Forschungsgemeinschaft*.

## References

- Bendlin C., Volkmer R., 1995, A&AS 112, 371  
 Brown T. M., 1984, Sci 226, 687  
 Deubner F.-L., Fleck B., Schmitz F., Straus T., 1992, A&A 266, 560  
 Espagnet O., Muller R., Roudier T., et al., 1996, A&A 313, 297  
 Fisher R.A., 1950, Statistical Methods for Research Workers. Oliver and Boyd, 11th edition  
 Goldreich P., Murray N., Kumar P., 1994, ApJ 424, 466  
 Goode P.R., Strous L.H., Rimmele T.R., Stebbins R.T., 1998, ApJ 495, L27  
 Kiefer M., 1999, Ph.D. Thesis, Albert-Ludwigs-Universität Freiburg i.B.  
 Kiefer M., Balthasar H., 1998, A&A 335, L73  
 Kiefer M., Grabowski U., Mattig W., Stix M., 2000, A&A 355, 381  
 Kim Y.-C., Chan K.L., 1998, ApJ 496, L121  
 Landau L.D., Lifshitz E.M., 1963, Course of theoretical physics. Vol. VI: Hydrodynamics. Pergamon, 2nd edition  
 Rast M.P., 1999, ApJ 524, 462  
 Rimmele T.R., Goode P.R., Harold E., Stebbins R.T., 1995, ApJ 444, L119  
 Stein R.F., Nordlund A., 1998, ApJ 499, 914  
 Stix M., 1991, The Sun, An Introduction. Springer-Verlag  
 Stix M., 2000, Solar Phys., submitted  
 Stix M., Zhugzhda Y., 1996, In: Pallavicini R., Dupree A.K. (eds.) 9th Cambridge Workshop on: Cool Stars, Stellar Systems, and the Sun. Vol. 109 of ASP Conference Series, p. 163  
 Stix M., Zhugzhda Y.D., 1998, A&A 335, 685  
 Zhugzhda Y.D., Stix M., 1994, A&A 291, 310